Supplemental Material

Supplementary Information for "Diagnosing mechanisms of hydrologic change under global warming in the CESM1 Large Ensemble"

Nicholas Siler,[a] David B. Bonan,[b] and Aaron Donohoe[c]

[a] *College of Earth, Ocean, and Atmospheric Sciences, Oregon State University, Corvallis, Oregon*

[b] *California Institute of Technology, Pasadena, California*

[c] *Polar Science Center/Applied Physics Lab, University of Washington, Seattle, Washington*

Corresponding author: Nicholas Siler, nick.siler@oregonstate.edu

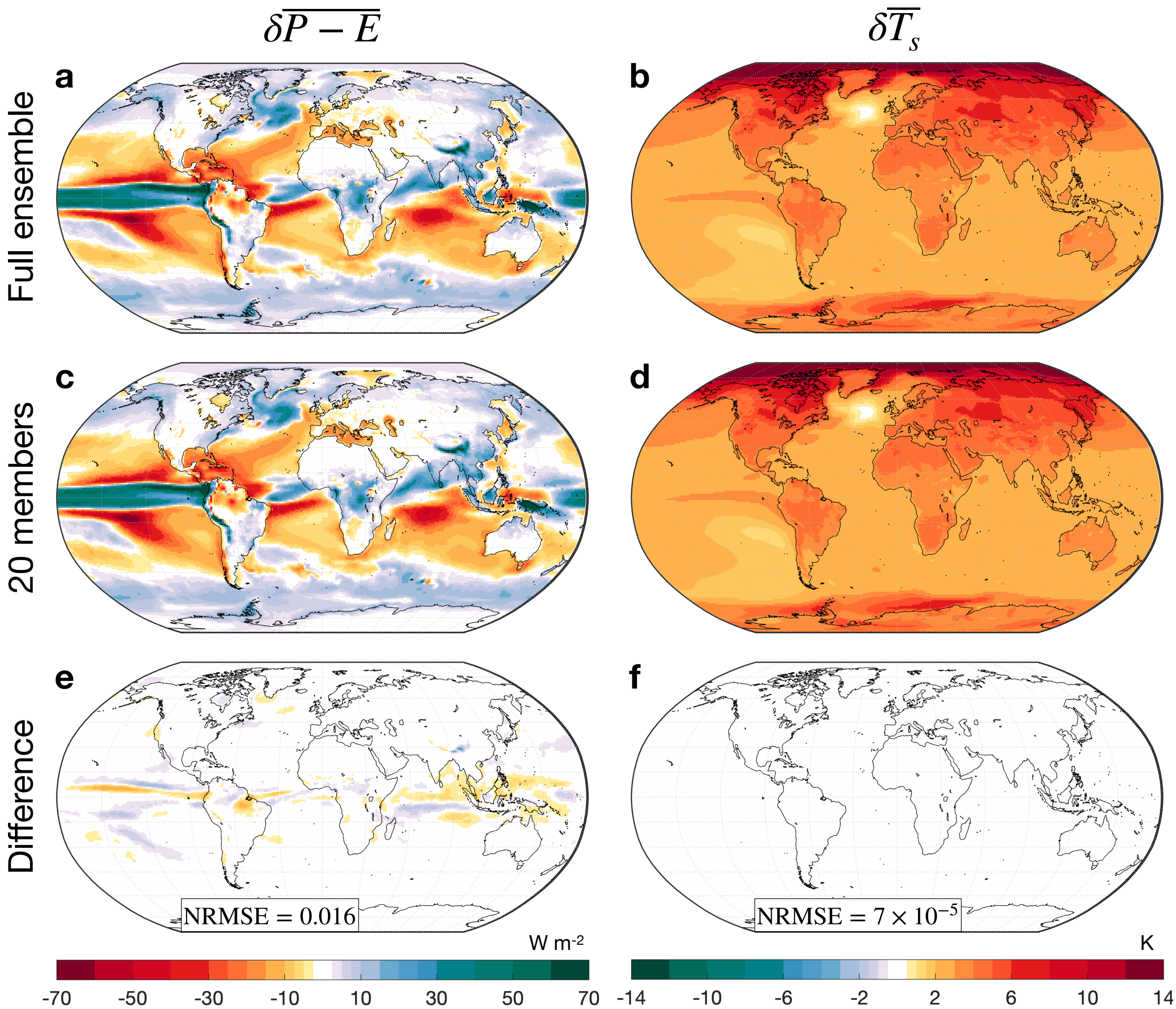

FIG. 1. a) The change in annual-mean, ensemble-mean precipitation minus evaporation ($\delta\overline{P-E}$) between 1991-2000 and 2071-2080 simulated by all 40 members of the CESM1 Large Ensemble. b) As in (a), but for the change in surface temperature ($\delta\overline{T_s}$). c-d) As in (a-b), but among the first 20 ensemble members. e-f) The difference between the changes in the full ensemble and those in the 20-member subset. The normalized root mean squared error (NRMSE), shown in the bottom left of (e) and (f), represents the square root of the sum of the squared differences divided by the square root of the sum of the squared changes. It is equal to 1.6% in (e) and 0.007% in (f), implying that the ensemble mean of the first 20 ensemble members is a good approximation of the total ensemble mean.

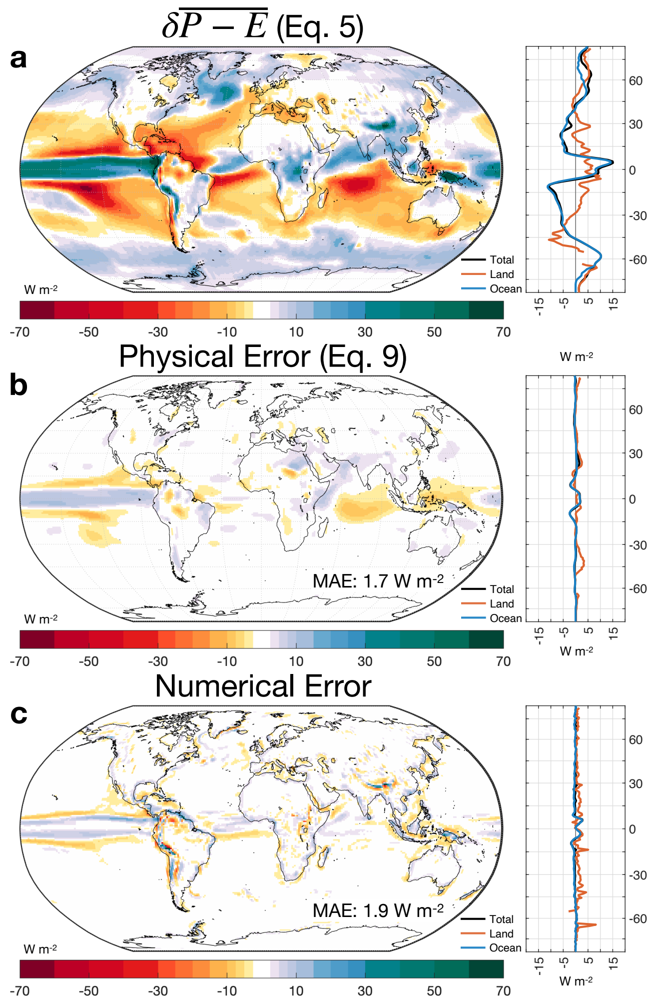

FIG. 2. a) $\delta\overline{P-E}$ computed numerically from 6-hourly q and $\mathbf{u}$ using Eq. 5 from the main manuscript. b) The physical component of the error in our decomposition of $\delta\overline{P-E}$, given by Eq. 9 in the main manuscript, which has a mean absolute value of 1.7 W m^{-2} (i.e., mean absolute error, or MAE). This is analogous to Fig. 3d in the main manuscript, but with the residual error computed relative to the pattern of $\delta\overline{P-E}$ in (a) instead of the true pattern of $\delta\overline{P-E}$ shown in Fig. 1b of the main manuscript. c) The numerical component of the error in our decomposition, which exhibits a MAE of 1.9 W m^{-2}. The numerical error is largest in the deep tropics and in high mountain ranges such as the Andes and Himalaya. The sum of (b) and (c) gives the total error shown in Fig. 3d in the main manuscript.

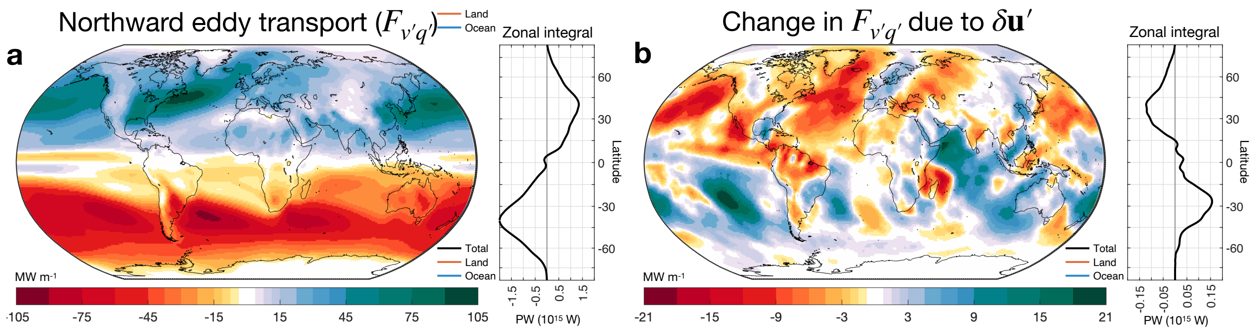

FIG. 3. a) The northward component of total column-integrated latent heat transport by eddies ($F_{v'q'}$) over the decade 1991-2000, in MW m^{-1} (10^{15} W m^{-1}). b) The change in $F_{v'q'}$ between the decades 1991-2000 and 2071-2080 that can be attributed to changes in transient winds ($\delta\mathbf{u}'$).

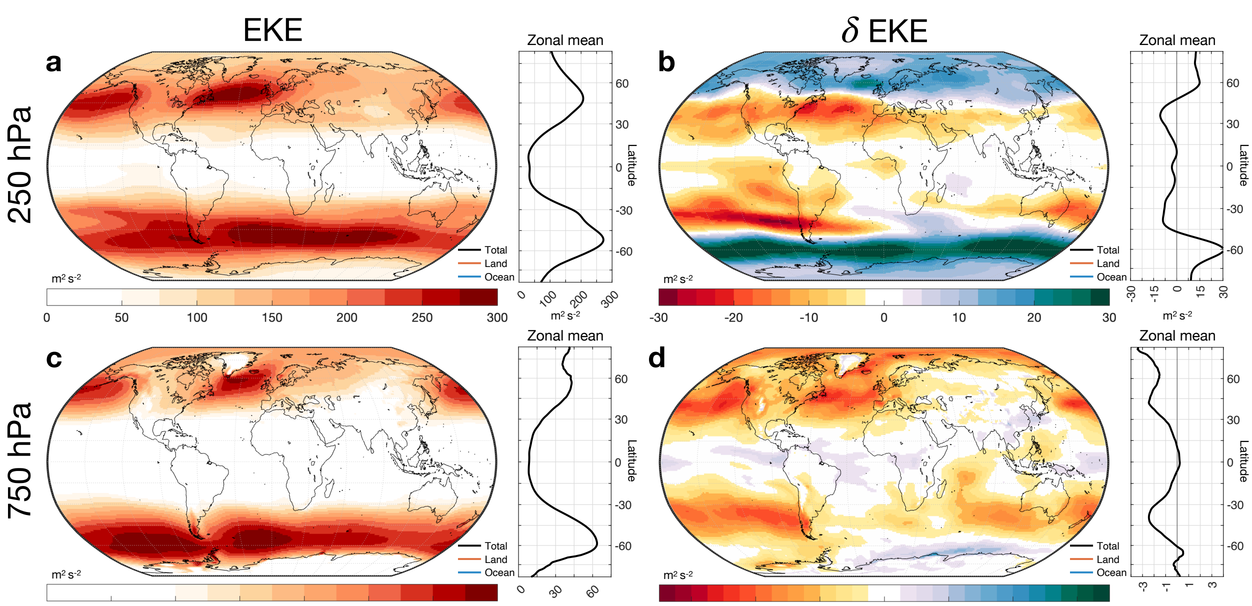

FIG. 4. a) Annual-mean eddy kinetic energy (EKE; in m^{2}s^{-2}) at 250 hPa over the decade 1991-2000, computed from wind anomalies relative to the mean for each month of each simulation. b) The change in annual-mean EKE at 250 hPa between the decades 1991-2000 and 2071-2080. c-d) As in (a-b), but at 750 hPa.

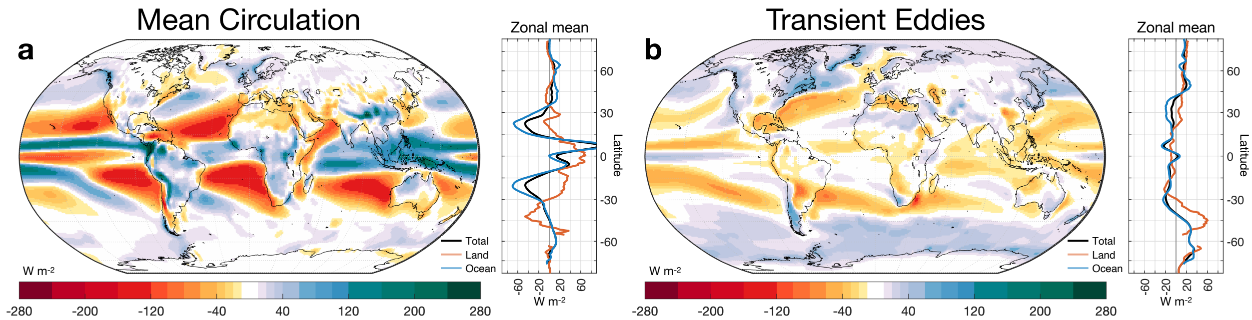

FIG. 5. A decomposition of annual-mean, ensemble-mean $P-E$ into contributions from (a) the mean circulation ($\overline{\bar{q}\bar{\mathbf{u}}}$) and from (b) transient eddies ($\overline{q'\mathbf{u}'}$), computed from 6-hourly q and $\mathbf{u}$ using Eq. 11 from the main manuscript.

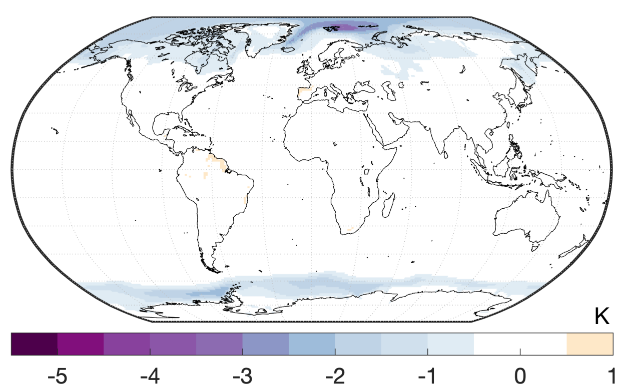

FIG. 6. The change in the annual-mean, ensemble-mean standard deviation (relative to monthly-means) of near-surface air temperature between 1991-2000 and 2071-2080. The magnitude of the change is at most a few K—much less than the inverse of the Clausius-Clapeyron scaling factor, $\alpha^{-1} = R_v T^2/L_v$, which ranges from about 12 K at high latitudes to 17 K in the tropics. The decrease in standard deviation at high latitudes is likely the result of eddies mixing across weakened temperature gradients due to polar-amplified warming (Supplementary Fig. 1b).

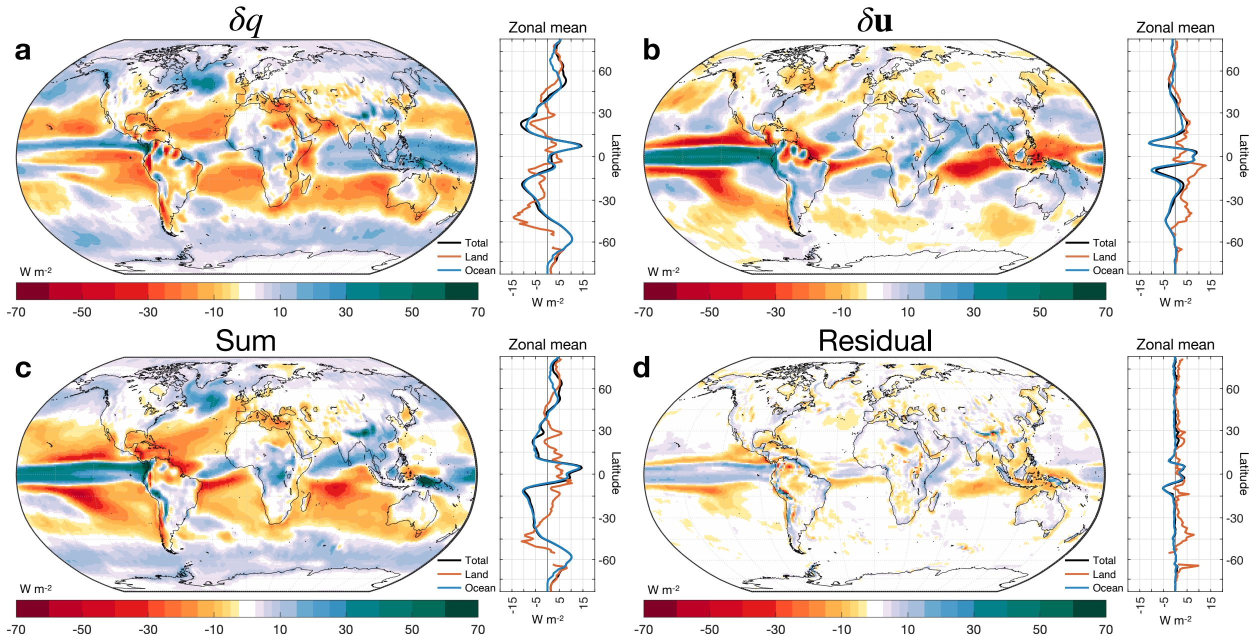

FIG. 7. As in Fig. 3 from the main text, but using only the first 10 members of the CESM-LE.